# Stability Assessment of a System Comprising a Single Machine and a Virtual Oscillator Controlled Inverter with Scalable Ratings

Mohammed Masum Siraj Khan, Yashen Lin
Power Systems Engineering Center
National Renewable Energy Laboratory
Email: {mohammed.khan, yashen.lin}@nrel.gov

Brian Johnson
Department of Electrical Engineering
University of Washington
Email: brianbj@uw.edu

Mohit Sinha, Sairaj Dhople
Department of ECE
University of Minnesota
Email: {sinha052, sdhople}@umn.edu

***Abstract*—We present a small-signal stability study of a coupled synchronous generator and inverter system, where the inverter is controlled by virtual oscillator control (VOC). VOC is a recently proposed grid-forming inverter control strategy, which acts on faster time scales compared to droop control. In our study, we leverage a scalable VOC controller (that is by design agnostic of power levels) to test the system's small-signal stability at different inverter penetration levels. The impact of rotational inertia, reactive power support, and filter parameters on stability is then investigated. Results highlight possible issues that might arise in these mixed machine-inverter systems further motivating the need to develop next generation stabilizing grid-forming controllers.**

## I. Introduction

As most renewable resources inject power via inverters, and are therefore markedly different from the traditional bulk power system because of the loss of rotational inertia, maintaining low-inertia stability poses a significant challenge and one which has garnered a lot of attention [1]–[7]. Control techniques proposed for these power electronic interfaces can be divided into two broad categories: i) grid-forming, and ii) grid-following. Grid-forming strategies refer to the paradigm where the power-electronic inverters dictate the voltage and frequency profiles based on the active and reactive power flows in the power network [8], [9], while in grid-following strategies, inverters operate to follow the voltage and frequency of the bus to which they are connected [10] through a phase-locked loop (PLL). To facilitate the transition towards a low-inertia system, it is imperative to perform the stability assessment of these control techniques in presence of machines as the migratory phase should continue to serve the demands that the electricity infrastructure meets without impediment. To this end, we present a stability study of a mixed machine and inverter setup to evaluates a recent suite of grid-forming methods called virtual oscillator control (VOC) [11], [12] that have been proposed to control voltage source inverters.

VOC is implemented by programming nonlinear differential equations for a class of nonlinear oscillators on the inverter micro-controllers to generate the pulse width modulation signal for the inverter switches. Fast dynamic performance, decentralized operation (which is robust and modular), and stability guarantees (for standalone systems) make it a compelling strategy for power systems with renewable resources [13]. This paper studies the impact of high renewable energy penetration on the transient stability of a power system when VOC is used for controlling inverters. It complements the previous stability assessment carried out in [14] and demonstrates the gap VOC could fill over conventional PLL-based grid following inverter control strategies while raising a few shortcomings that need to be addressed to further improve VOC. Our simplified problem setup is chosen to be similar to the one in [14]—a single machine connected to an inverter serving a load—in order to highlight the role of machine inertia, filter parameters, and reactive power support in maintaining small-signal stability. A schematic of the system is shown in Fig. 1. A complex system with a larger number of inverters and synchronous generators that interact over a distribution network is more realistic; however due to the large number of dynamic states involved, it is hard to clearly highlight the roles of the aforementioned quantities. Therefore, this study intends to be foundational with the understanding that insights derived here could be leveraged to analyze more complex setups.

To establish the stability of the coupled machine-inverter system, we linearize the differential algebraic equation model that emerges from the power flow equations along with the intrinsic dynamics of the machine and inverter, following which we compute the eigenvalues of the linearized system. Similar to [14], we leverage a set of scaling laws to design VOC for different power ratings that presents consistent dy-

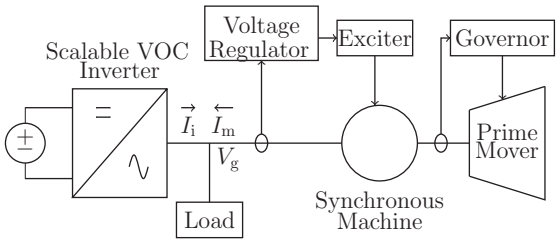


Fig. 1: Model of a single-machine and single-inverter system, where the power and voltage of the inverter are scalable.

978-1-5090-6684-1/18/$31.00 ©2018 IEEE

namic behavior and represents an aggregation of many such oscillator-controlled inverters. We consider different variations, namely: inverter penetration level (defined to be the ratio of the power rating of the inverter to the power rating of the system), reactive power ratings, the machine inertia constant, and parametric variations in the inverter filters, and look at the trends of the spectrum of the linearized system.

The remainder of this paper is organized as follows. The scalable VOC inverter and machine models are introduced in Section II. Small-signal stability analysis via numerical simulation is then carried out in Section III. Finally, Section IV draws conclusions and highlights a few key directions for future work.

## II. Scalable VOC-Inverter And Machine Model

In this section, we introduce the dynamical models of the VOC controlled inverter and machine in their local $\mathrm{dq}$ reference frames along with the electrical network model that couples both the systems. Subsequently, the impact of inverter power penetration level, control parameters, and machine inertia on system small-signal stability is examined.

### A. Machine Model

We begin with a brief overview of the model we use for a steam-driven generator that consists of a synchronous machine, exciter, governor, and prime mover. (We refer interested readers to [15] for further details.) The model dynamics can be expressed compactly as:

$$\dot{x}_{\mathrm{m}} = f_{\mathrm{m}}(x_{\mathrm{m}}, u_{\mathrm{m}}), \tag{1}$$

with the following states and inputs:

$$x_{\mathrm{m}} = [\delta_{\mathrm{g}}, \omega, P_{\mathrm{g}}, P_{\mathrm{gt}}, P_{\mathrm{m}}, v_{\mathrm{c}}, v_{\mathrm{fd}}, \lambda_{\mathrm{fd}}]^{\top}, \tag{2}$$

$$u_{\mathrm{m}} = [P_{\mathrm{agc}}, v^{*}, i_{\mathrm{m}}^{\mathrm{dq}}]^{\top}, \tag{3}$$

where $\delta_{\mathrm{g}}$ is the rotor angle (that establishes the $\mathrm{dq}$ reference frame), $\omega$ is the frequency, $P_{\mathrm{g}}$ is the governor output, $P_{\mathrm{gt}}$ is an internal steam-turbine state, $P_{\mathrm{m}}$ is the mechanical power driving the rotor, $v_{\mathrm{c}}$ is the voltage controller output, $v_{\mathrm{fd}}$ is the exciter field voltage, and $\lambda_{\mathrm{fd}}$ is the field flux linkage. The inputs consist of the AGC reference signal, $P_{\mathrm{agc}}$, the terminal voltage command, $v^{*}$, and the machine terminal currents $i_{\mathrm{m}}^{\mathrm{dq}} = [i_{\mathrm{m}}^{\mathrm{d}}, i_{\mathrm{m}}^{\mathrm{q}}]^{\top}$. In essence, the model consists of a frequency loop that describes the rotor dynamics and a voltage loop that captures the electromagnetic field equations. Figure 2 illustrates the frequency- and voltage-control loops. In the following sections, we denote the machine power rating as $P_{\mathrm{m}}$ and all relevant model parameters, inputs, and states are converted to per-unit using the machine power and voltage ratings as base values [15].

### B. Dynamic Model of Scalable VOC Inverter

Figure 3 illustrates the model for a scalable three-phase VOC inverter [11], [12]. In order to scale the VOC inverter to the required power and voltage ratings, two scaling factors (power and voltage) denoted by $\mu_{\mathrm{p}}$ and $\mu_{\mathrm{v}}$ are introduced. Before getting into details of the scaled-VOC inverter dynamics,

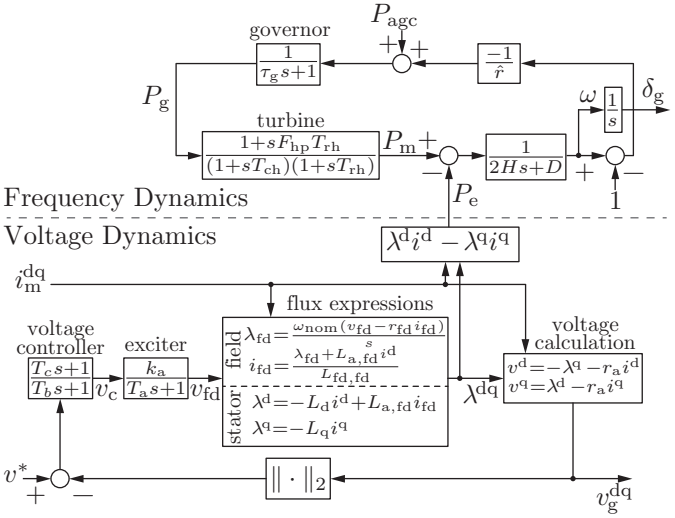


Fig. 2: Block diagram of synchronous-machine electromechanical dynamics [14].

the dynamical model of the unscaled VOC inverter (where the power and voltage scaling factors, $\mu_{\mathrm{p}} = \mu_{\mathrm{v}} = 1$) is described.

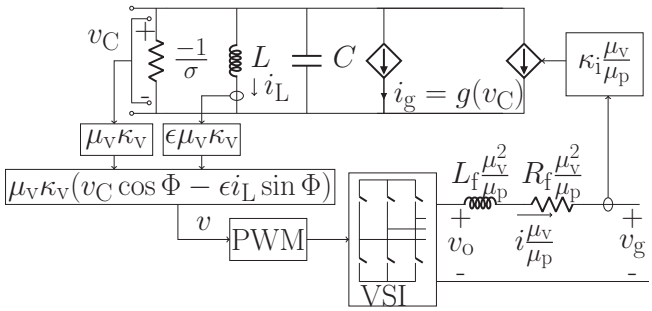


Fig. 3: Diagram of scalable model for a single inverter with VOC, where $\mu_{\mathrm{p}}$ and $\mu_{\mathrm{v}}$ are the power and voltage scaling factors, respectively.

*1) Unscaled VOC Inverter model:* The closed-loop virtual oscillator controller is implemented by programming a second-order nonlinear differential equation on the inverter microcontroller. The dynamics also admit a circuit representation and the resulting oscillator circuit can be seen to be a parallel combination of the following elements: i) a harmonic oscillator with the capacitance, $C$, inductance, $L$, with the resonant frequency, $\omega_{\mathrm{nom}} = 1/\sqrt{LC}$, ii) a negative conductance element, $-\sigma$, iii) a cubic voltage-dependent current source, $g(v_{\mathrm{C}}) = \alpha v_{\mathrm{C}}^{3}$, where $v_{\mathrm{C}}$ is the voltage across the capacitor, and $\alpha$ is a positive real constant. The virtual oscillator is coupled to the physical signals of the inverter through the voltage and current rating factors, $\kappa_{\mathrm{v}}$ and $\kappa_{\mathrm{i}}$, respectively. In particular, the inverter output current, $i$, is multiplied by the current rating factor, $\kappa_{\mathrm{i}}$, and the signal, $\kappa_{\mathrm{i}} i$, is passed to the virtual oscillator circuit. The output voltage, $v_{\mathrm{C}}$, across the virtual capacitor ($C$) is multiplied by the voltage rating factor, $\kappa_{\mathrm{v}}$, and the virtual inductor current, $i_{\mathrm{L}}$, is multiplied by $\epsilon\kappa_{\mathrm{v}}$ where $\epsilon = \sqrt{L/C}$. Finally the signals ($v_{\mathrm{C}}\kappa_{\mathrm{v}}$, and $i_{\mathrm{L}}\epsilon\kappa_{\mathrm{v}}$) are used to construct

the reference signal, $v$, which is used to generate the PWM signal. The inverter is connected to the machine through the $RL$ output filter which has an inductance, $L_{\rm f}$ and a resistance, $r_{\rm f}$. The dynamical equations of the virtual-oscillator inductor current, $i_{\rm L}$, and capacitor voltage, $v_{\rm C}$, are [12]:

$$L\frac{di_{\rm L}}{dt} = v_{\rm C},\ C\frac{dv_{\rm C}}{dt} = -\alpha v_{\rm C}^3 + \sigma v_{\rm C} - i_{\rm L} - \kappa_{\rm i} i. \tag{4}$$

The output voltage, $v$, of the virtual-oscillator is given by

$$v = \kappa_{\rm v}(v_{\rm C}\cos\Phi - \epsilon i_{\rm L}\sin\Phi), \tag{5}$$

where $\Phi$ is a fixed user-defined angle, typically chosen as either 0 or $\pi/2$. The value of $\Phi$ determines the droop-like characteristics of the VO-controlled inverter in steady-state [12]. In this paper the value of $\Phi$ is chosen as $\Phi = \pi/2$ so that the VOC inverter exhibits the $\omega$-versus-$p$ and $V$-versus-$q$ droop-like relationships.

The averaged dynamical model governing the terminal voltage and frequency dynamics is given by [11]:

$$\dot{V} = \frac{\sigma}{2C}(V - \frac{\beta}{2}V^3) - \frac{k_{\rm i}k_{\rm v}}{2CV}Q, \tag{6}$$

$$\dot{\delta}_{\rm i} = \omega_{\rm i} = \omega_{\rm nom} - \frac{k_{\rm i}k_{\rm v}}{2CV^2}P, \tag{7}$$

where $\beta = 3\sigma/(k_{\rm v}^2\sigma)$, and $P$ and $Q$ are average real and reactive power outputs. The average real and reactive power are computed using unfiltered signals (8) as VOC is a time-domain controller and the average model of the VOC inverter incorporates no additional filters:

$$\begin{bmatrix} P \\ Q \end{bmatrix} = \begin{bmatrix} V & 0 \\ 0 & -V \end{bmatrix} \begin{bmatrix} i_{\rm l}^{\rm d} \\ i_{\rm l}^{\rm q} \end{bmatrix}. \tag{8}$$

Using relation (8) in (6) and (7), we have:

$$\dot{V} = \frac{\sigma}{2C}(V - \frac{\beta}{2}V^3) + \frac{k_{\rm i}k_{\rm v}}{2C}i_{\rm l}^{\rm q}, \tag{9}$$

$$\dot{\delta}_{\rm i} = \omega_{\rm i} = \omega_{\rm nom} - \frac{k_{\rm i}k_{\rm v}}{2CV}i_{\rm l}^{\rm d}. \tag{10}$$

The dynamics of the inverter output filter are given by [13]:

$$\dot{i}_{\rm l}^{\rm d} = \frac{1}{L_{\rm f}}(-r_{\rm f}i_{\rm l}^{\rm d} + v_{\rm o}^{\rm d} - v_{\rm g}^{\rm d}) + \omega_{\rm i}i_{\rm l}^{\rm q}, \tag{11}$$

$$\dot{i}_{\rm l}^{\rm q} = \frac{1}{L_{\rm f}}(-r_{\rm f}i_{\rm l}^{\rm q} + v_{\rm o}^{\rm q} - v_{\rm g}^{\rm q}) - \omega_{\rm i}i_{\rm l}^{\rm d}. \tag{12}$$

Since the model is in the inverter reference frame, we note that $[v_{\rm o}^{\rm d}, v_{\rm o}^{\rm q}]^\top = [V, 0]^\top$. Then, (11) and (12) simplify to

$$\dot{i}_{\rm l}^{\rm d} = \frac{1}{L_{\rm f}}(-r_{\rm f}i_{\rm l}^{\rm d} + V - v_{\rm g}^{\rm d}) + \omega_{\rm i}i_{\rm l}^{\rm q}, \tag{13}$$

$$\dot{i}_{\rm l}^{\rm q} = \frac{1}{L_{\rm f}}(-r_{\rm f}i_{\rm l}^{\rm q} - v_{\rm g}^{\rm q}) - \omega_{\rm i}i_{\rm l}^{\rm d}. \tag{14}$$

The dynamical model of the unscaled VOC inverter is given by equations (9), (10), (13), (14). In concise form, it can be written as:

$$\dot{x}_{\rm i} = f_{\rm i}(x_{\rm i}, u_{\rm i}), \tag{15}$$

where $x_{\rm i}$ and $u_{\rm i}$ represent the dynamical states and inputs respectively, and they are listed below:

$$x_{\rm i} = [i_{\rm l}^{\rm d}, i_{\rm l}^{\rm q}, v_{\rm o}^{\rm d}, v_{\rm o}^{\rm q}, \delta_{\rm i}]^\top, \tag{16}$$

$$u_{\rm i} = [v_{\rm g}^{\rm d}, v_{\rm g}^{\rm q}]^\top. \tag{17}$$

*2) Parameter design:* In this section, we briefly describe the design procedure of the VOC parameters, which is based on [11]. First, we choose the voltage rating factor, $\kappa_{\rm v}$ and current rating factor, $\kappa_{\rm i}$, as follows:

$$\begin{aligned} \kappa_{\rm v} &:= V_{\rm oc}, \\ \kappa_{\rm i} &:= \frac{V_{\min}}{|Q_{\rm rated}|}, \end{aligned} \tag{18}$$

where $V_{\rm oc}$ is the open-circuit voltage of the inverter, $V_{\min}$ is the minimum voltage allowed, and $|Q_{\rm rated}|$ is the rated reactive power output of the inverter. With this choice, the VO capacitor voltage is 1V RMS when the inverter terminal voltage is equal to the open-circuit voltage $V_{\rm oc}$, and the VO output current is 1A when the inverter is providing its full rated reactive power $|Q_{\rm rated}|$.

Next we choose $C, \sigma, \alpha$ so that the maximum allowed frequency droop $|\Delta\omega|_{\max}$ is achieved at $P_{\rm rated}$, and the minimum voltage allowed $V_{\min}$ is achieved at $|Q_{\rm rated}|$. This leads to the following:

$$\sigma := \frac{V_{\rm oc}}{V_{\min}}\frac{V_{\rm oc}^2}{V_{\rm oc}^2 - V_{\min}^2}, \tag{19}$$

$$\alpha := \frac{2\sigma}{3}, \tag{20}$$

$$C := \frac{1}{2|\Delta\omega|_{\max}}\frac{V_{\rm oc}}{V_{\min}}\frac{P_{\rm rated}}{|Q_{\rm rated}|}. \tag{21}$$

Lastly, the value of the VO inductance is calculated as:

$$L = \frac{1}{C(\omega_{\rm nom})^2}. \tag{22}$$

*3) Scaling law for the VOC Inverter model:* Now, we describe how the controlled parameters of the VOC inverter can be systematically tuned to obtain a model for a desired power level and terminal voltage. Define the power and voltage ratings of the scaled inverter as follows:

$$P_{\rm s} := \mu_{\rm p}P,\ V_{\rm s} := \mu_{\rm v}V, \tag{23}$$

where $\mu_{\rm p}$ and $\mu_{\rm v}$ are the power and voltage scaling factors, and $P$ and $V$ are the power and voltage ratings of the unscaled inverter, respectively. Furthermore, let $k_{\rm v,s}$ and $k_{\rm i,s}$ be the scaled voltage gain, and current factor, respectively, and let $L_{\rm f,s}$, $r_{\rm f,s}$ be the scaled filter parameters for the inverter, whose values are given by:

$$\begin{aligned} k_{\rm v,s} &:= \mu_{\rm v}k_{\rm v},\ k_{\rm i,s} := \frac{\mu_{\rm v}}{\mu_{\rm p}}k_{\rm i}, \\ L_{\rm f,s} &:= \frac{\mu_{\rm v}^2}{\mu_{\rm p}}L_{\rm f},\ r_{\rm f,s} := \frac{\mu_{\rm v}^2}{\mu_{\rm p}}r_{\rm f}. \end{aligned} \tag{24}$$

### C. Combined Machine and Inverter Model

To combine the machine and inverters models, we need to describe the system in a common reference frame as well as have a consistent system of units. To that end, we first transform the VOC inverter model into per unit using the machine base and then leverage a coordinate transformation to convert the machine terminal variables to the inverter $\mathrm{dq}$ reference frame as follows:

$$\begin{bmatrix} x_{\mathrm{m}}^{\mathrm{d}} \\ x_{\mathrm{m}}^{\mathrm{q}} \end{bmatrix} = \begin{bmatrix} \cos(\omega_{\mathrm{nom}}(\delta_{\mathrm{g}} - \delta_{\mathrm{i}})) & -\sin(\omega_{\mathrm{nom}}(\delta_{\mathrm{g}} - \delta_{\mathrm{i}})) \\ \sin(\omega_{\mathrm{nom}}(\delta_{\mathrm{g}} - \delta_{\mathrm{i}})) & \cos(\omega_{\mathrm{nom}}(\delta_{\mathrm{g}} - \delta_{\mathrm{i}})) \end{bmatrix} \begin{bmatrix} x_{\mathrm{m}}^{\mathrm{D}} \\ x_{\mathrm{m}}^{\mathrm{Q}} \end{bmatrix}. \tag{25}$$

Above, variables superscripted with $\mathrm{d}$ and $\mathrm{q}$ are in the inverter $\mathrm{dq}$ reference frame and variables superscripted with $\mathrm{D}$ and $\mathrm{Q}$ are in the machine reference frame. Machine-inverter angle difference, $\delta := \delta_{\mathrm{g}} - \delta_{\mathrm{i}}$, is used to establish the common frame of reference where all variables are represented. From Kirchhoff's law,

$$V_{\mathrm{g}} = z(I_{\mathrm{m}} + I_{\mathrm{i}}), \tag{26}$$

where $z$ is the load impedance, $V_{\mathrm{g}} = v_{\mathrm{g}}^{\mathrm{d}} + j v_{\mathrm{g}}^{\mathrm{q}}$, $I_{\mathrm{m}} = i_{\mathrm{m}}^{\mathrm{d}} + j i_{\mathrm{m}}^{\mathrm{q}}$, and $I_{\mathrm{i}} = i_{\mathrm{l}}^{\mathrm{d}} + j i_{\mathrm{l}}^{\mathrm{q}}$ are the machine terminal voltage, machine terminal current, and inverter terminal current, respectively. From (25) and (26), we obtain the following general algebraic equation that describes the electrical network coupling constraint between the machine and the inverter state variables:

$$0 = g(i_{\mathrm{m}}^{\mathrm{d}}, i_{\mathrm{m}}^{\mathrm{q}}, i_{\mathrm{l}}^{\mathrm{d}}, i_{\mathrm{l}}^{\mathrm{q}}, v_{\mathrm{g}}^{\mathrm{d}}, v_{\mathrm{g}}^{\mathrm{q}}, \delta_{\mathrm{g}} - \delta_{\mathrm{i}}). \tag{27}$$

Finally, the solution of network equation (27) can be used to express the internal input variables ($v_{\mathrm{g}}^{\mathrm{dq}}$, $i_{\mathrm{m}}^{\mathrm{dq}}$) in terms of the state variables ($\lambda_{\mathrm{fd}}$, $i_{\mathrm{o}}^{\mathrm{dq}}$, $\delta_{\mathrm{g}} - \delta_{\mathrm{i}}$) and upon their elimination, we get a dynamical system representation of the form:

$$\dot{x} = f(x, u), \tag{28}$$

where $x$ represents all the dynamical states of the machine and the inverter as given in (2) and (16), respectively and $u$ captures all the inputs of the system.

## III. Small-signal Stability Analysis

Having establishing the coupled model of the machine and inverter, we test the small-signal stability of the system across different inverter penetration levels. Consider a system with a total capacity $P_{\mathrm{sys}}$, which is served by a scalable VOC inverter rated at $P_{\mathrm{inv}}$ and a synchronous machine rated at $P_{\mathrm{m}}$, i.e., $P_{\mathrm{sys}} = P_{\mathrm{m}} + P_{\mathrm{inv}}$. Define the inverter penetration level as:

$$r = \frac{P_{\mathrm{inv}}}{P_{\mathrm{sys}}}. \tag{29}$$

When sweeping across different values of $r$, we keep the system capacity fixed and increase the inverter rating to study its impacts on system stability. This emulates the scenario where inverter based sources gradually replace synchronous machines in the system. As the inverter rating changes, its model parameters are scaled accordingly as discussed in Section II-B. We assume that the per unit parameters of the machine base do not change as the machine rating changes. The base values change according to the rating change, capturing the physical parameter changes as the size of the machine changes.

At each penetration level, we evaluate small-signal stability. We linearize the system dynamics (28) around the equilibrium point $(x^*, u^*)$ [14],

$$\Delta\dot{x} = A\Delta x + B\Delta u, \tag{30}$$

where $A := \frac{\partial f}{\partial x}|_{(x^*,u^*)}$ and $B := \frac{\partial f}{\partial u}|_{(x^*,u^*)}$. Then we calculate the eigenvalues of the matrix $A$ to determine the small-signal stability of the system.

### A. Test system parameters

The system's rating is $P_{\mathrm{sys}} = 650\mathrm{MW}$ and $Q_{\mathrm{sys}} = 300\mathrm{MVAR}$ at the nominal voltage. The power rating of the machine is $P_{\mathrm{m}} = 555\mathrm{MW}$, the line-to-line voltage rating is 24kV, and the nominal frequency is $\omega_{\mathrm{nom}} = 2\pi \times 60$ rad/s. The relevant parameters of the machine are given in Table I [15]. For the unscaled VOC inverter, we adopted the parameters from [13]; shown in Table II.

TABLE I: Parameters of the machine model, values are in per unit unless specified otherwise.

| | | |
|---|---|---|
| $H = 2.9\mathrm{s}$ | $D = 1$ | $\hat{r} = 0.05$ |
| $\tau_{\mathrm{g}} = 0.2\mathrm{s}$ | $F_{\mathrm{hp}} = 0.3$ | $T_{\mathrm{rh}} = 7\mathrm{s}$ |
| $T_{\mathrm{ch}} = 0.3\mathrm{s}$ | $k_{\mathrm{a}} = 0.0745$ | $T_{\mathrm{a}} = 0.04\mathrm{s}$ |
| $T_{\mathrm{b}} = 12\mathrm{s}$ | $T_{\mathrm{c}} = 1\mathrm{s}$ | $R_{\mathrm{fd}} = 0.0006$ |
| $R_{\mathrm{a}} = 0.003$ | $L_{\mathrm{a,fd}} = 1.66$ | $L_{\mathrm{fd,fd}} = 1.825$ |
| $L_{\mathrm{d}} = 1.81$ | $L_{\mathrm{q}} = 1.76$ | $P_{\mathrm{agc}} = 0.9$ |

TABLE II: Virtual-oscillator control parameters.

| Symbol | Value | Units |
|---|---|---|
| $\kappa_{\mathrm{v}}$ | $120 \times 1.05$ | V/V |
| $\kappa_{\mathrm{i}}$ | 0.1520 | A/A |
| $\sigma$ | 6.0927 | $\Omega^{-1}$ |
| $\alpha$ | 4.0618 | $\mathrm{A/V}^3$ |
| $C$ | 0.1759 | F |
| $L$ | $3.99 \times 10^{-5}$ | H |
| $L_f$ | $1 \times 10^{-3}$ | H |
| $r_f$ | 0.7 | $\Omega$ |

### B. Stability Analysis

We first consider a base case, where the system parameters described in Section III-A are used. Next, we vary a few parameters to study their impact on system stability.

*1) Base Case:* For the base case, the small-signal stability results of the coupled machine-inverter system are shown in Fig. 4. We plot the real part of the right-most eigenvalue on the complex plane, $\max(\mathrm{Re}(\lambda))$, as a function of the penetration level $r$. The system is small-signal stable if $\max(\mathrm{Re}(\lambda))$ is negative, and unstable if $\max(\mathrm{Re}(\lambda))$ is positive. From Fig. 4, we observe that the small-signal stability is maintained when the inverter penetration level is low. When the penetration level increases, the system eventually becomes unstable. In this case, the tipping point is around 50%.

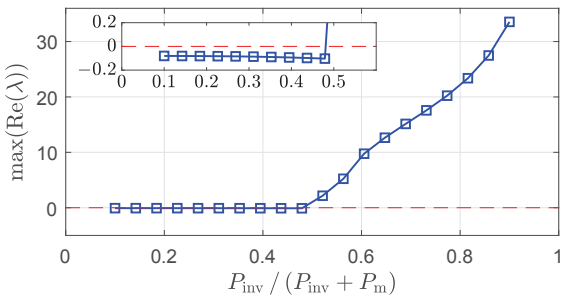


Fig. 4: Base case: small-signal stability analysis with the variation of inverter penetration.

We conjecture that the instability is related to the reactive power output from the inverter. Recall from (6) that the VOC controller has a $V$-$q$ droop-like behavior. Taking a first order expansion of $V$ around the open-circuit voltage $V_{\text{oc}}$, we get the standard droop form:

$$V_{\text{eq}} = V_{\text{oc}} + m_{\text{Q}} Q_{\text{eq}}, \tag{31}$$

where the droop gain is given by:

$$m_{\text{Q}} = \frac{\kappa_{\text{v}} \kappa_{\text{i}}}{2\sigma} \left( V_{\text{oc}} - \beta V_{\text{oc}}^3 \right)^{-1}. \tag{32}$$

Recall from Section II-B where we list the choice of $\kappa_{\text{v}}, \kappa_{\text{i}}, \sigma, \beta$, that as we increase the inverter penetration level, the rating $Q_{\text{rated}}$ increases, and the droop gain $m_{\text{Q}}$ becomes smaller. This means a small deviation from the open-circuit voltage leads to significant reactive power output from the inverter. This excessive reactive power injection could lead to instability in the system.

*2) Impact of Inverter Reactive Power Droop Slope:* To further study the impact of reactive power on system stability, we evaluated the system with different inverter reactive power droop slopes. In the base case, the inverter reactive power rating is the same as its active power rating, i.e., $|Q_{\text{rated}}| = P_{\text{rated}}$. In this section, we consider two other scenarios: $|Q_{\text{rated}}| = 0.5 \times P_{\text{rated}}$ and $|Q_{\text{rated}}| = 0.1 \times P_{\text{rated}}$. The results are shown in Fig. 5. We observed that the stable region is increased as the inverter reactive power rating decreases.

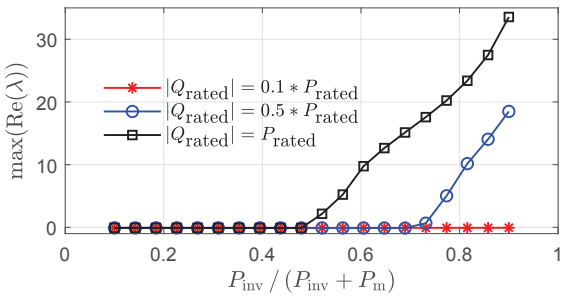


Fig. 5: Stability results with different inverter reactive power ratings.

The obvious trade-off in this improvement of stability is the reduction in reactive power the inverter can provide. The dynamical performance of the inverter is also affected by the change of reactive power rating. From [11], the rise time of voltage is approximated by:

$$t_r \approx \frac{6}{\sigma} C. \tag{33}$$

Recall from (33) that when $|Q_{\text{rated}}|$ reduces, $C$ increases, leading to a longer rise time.

*3) Impact of Machine Inertia:* We also studied the impact of machine inertia on system stability by scaling the inertia $M$ by a factor of 100 and 0.1. The results are shown in Fig. 6, where we observed when the machine inertia varies, the magnitude of the eigenvalue varies, but the tipping point where the system becomes unstable is not significantly changed.

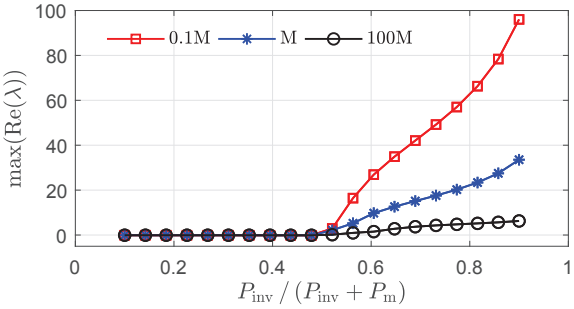


Fig. 6: Stability assessment with the scalable machine inertia.

*4) Impact of Filter Parameters:* Next we studied the impact of the inverter output filter. We scaled $L_{\text{f,s}}$ and $r_{\text{f,s}}$ by a factor of 10 and 0.1. The results are shown in Fig. 7. We observed that when the filter parameters increases, the stable region also increases; while when the filter parameters decreases, there is no significant changes in system stability.

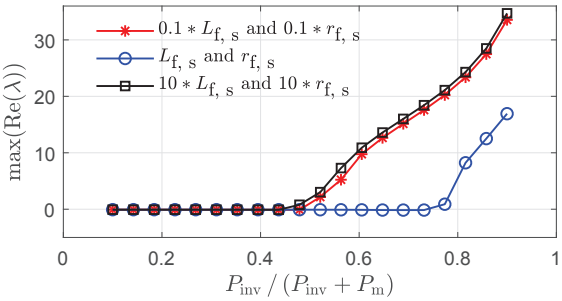


Fig. 7: Estimating the impacts of the scalable filter parameters on the small-signal stability of the system.

### C. Time Domain Validation

In order to validate the small-signal model with the perturbation of the load change, we consider two time-domain simulations with different penetration levels: a stable case where $r = 45\%$ and $\max(\text{Re}(\lambda))$ is negative, and an unstable case where $r = 55\%$ and $\max(\text{Re}(\lambda))$ is positive. We start the simulation at the equilibrium point, and introduce a 5% load change at $t = 2$s. The results are shown in Fig. 8. We observe

that in the $r = 45\%$ case, the time-domain signal settles down to a new steady state, while in the $r = 55\%$ case, the state diverges. These time domain simulation results are consistent with our small-signal stability analysis.

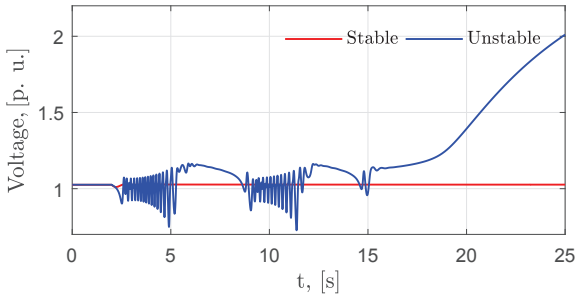


Fig. 8: Time domain simulation of the original nonlinear system for two different inverter penetration levels, $r = 0.45$ and $r = 0.55$, whose linearizations have positive and negative $\max(\mathrm{Re}(\lambda))$ respectively.

## IV. Conclusion and Future Work

In this paper, we evaluated the transient stability of a mixed machine and inverter system where the inverter was controlled using virtual oscillator control with an emphasis of the impact of the power penetration level of the inverter. To that end, we built an aggregated model of the inverter and machine in d-q coordinates and numerically computed eigenvalues of the linearized system. In particular, we examined the maximum real-part of the eigenvalues, the sign of which determines the stability of the system, against inverter penetration level for different reactive power ratings, filter parameters, and machine inertia constants to establish the efficacy of VOC and to highlight a few of its shortcomings that might inform further improvement. Implementing and validating the study in hardware is a part of ongoing investigations. Other revenues for future work include a more comprehensive sensitivity analysis, considering more advanced controllers in the model, and participation factor analysis.

## Acknowledgments

This work was supported in part by the: i) Alliance for Sustainable Energy, LLC, the Manager and Operator of the National Renewable Energy Laboratory for the U.S. Department of Energy (DOE) under Contract No. DE-AC36-08GO28308. Funding provided by U.S. Department of Energy Office of Energy Efficiency and Renewable Energy Solar Energy Technologies Office; and ii) National Science Foundation through grants 1453921 and 1509277. The views expressed in the article do not necessarily represent the views of the DOE or the U.S. Government. The U.S. Government retains and the publisher, by accepting the article for publication, acknowledges that the U.S. Government retains a nonexclusive, paid-up, irrevocable, worldwide license to publish or reproduce the published form of this work, or allow others to do so, for U.S. Government purposes.

## References

[1] F. Milano, F. Dörfler, G. Hug, D. J. Hill, and G. Verbic, "Foundations and challenges of low-inertia systems," in *20th Power System Computation Conference (PSCC), Dublin, Ireland*, 2018, pp. 11–15.

[2] A. Ulbig, T. S. Borsche, and G. Andersson, "Impact of low rotational inertia on power system stability and operation," *IFAC Proceedings Volumes*, vol. 47, no. 3, pp. 7290–7297, 2014.

[3] C. Kammer and A. Karimi, "Decentralized and distributed transient control for microgrids," *IEEE Transactions on Control Systems Technology*, pp. 1–12, 2017.

[4] T. Kerdphol, F. S. Rahman, Y. Mitani, M. Watanabe, and S. Kufeoglu, "Robust virtual inertia control of an islanded microgrid considering high penetration of renewable energy," *IEEE Access*, vol. 6, pp. 625–636, 2018.

[5] M. Ayar, S. Obuz, R. D. Trevizan, A. S. Bretas, and H. A. Latchman, "A distributed control approach for enhancing smart grid transient stability and resilience," *IEEE Transactions on Smart Grid*, vol. 8, no. 6, pp. 3035–3044, Nov 2017.

[6] K. De Brabandere, B. Bolsens, J. Van Den Keybus, J. Driesen, M. Prodanovic, and R. Belmans, "Small-signal stability of grids with distributed low-inertia generators taking into account line phasor dynamics," in *Electricity Distribution, 2005. CIRED 2005. 18th International Conference and Exhibition on*. IET, 2005, pp. 1–5.

[7] M. Pirani, J. W. Simpson-Porco, and B. Fidan, "System-theoretic performance metrics for low-inertia stability of power networks," in *Decision and Control (CDC), 2017 IEEE 56th Annual Conference on*. IEEE, 2017, pp. 5106–5111.

[8] T. Vandoorn, J. De Kooning, B. Meersman, and L. Vandevelde, "Review of primary control strategies for islanded microgrids with power-electronic interfaces," *Renewable and Sustainable Energy Reviews*, vol. 19, pp. 613–628, 2013.

[9] J. M. Carrasco, L. G. Franquelo, J. T. Bialasiewicz, E. Galván, R. C. PortilloGuisado, M. M. Prats, J. I. León, and N. Moreno-Alfonso, "Power-electronic systems for the grid integration of renewable energy sources: A survey," *IEEE Transactions on industrial electronics*, vol. 53, no. 4, pp. 1002–1016, 2006.

[10] A. Nicastri and A. Nagliero, "Comparison and evaluation of the pll techniques for the design of the grid-connected inverter systems," in *Industrial Electronics (ISIE), 2010 IEEE International Symposium on*. IEEE, 2010, pp. 3865–3870.

[11] B. B. Johnson, M. Sinha, N. G. Ainsworth, F. Dörfler, and S. V. Dhople, "Synthesizing virtual oscillators to control islanded inverters," *IEEE Transactions on Power Electronics*, vol. 31, no. 8, pp. 6002–6015, 2016.

[12] M. Sinha, S. Dhople, B. Johnson, N. Ainsworth, and F. Dörfler, "Nonlinear supersets to droop control," in *Control and Modeling for Power Electronics (COMPEL), 2015 IEEE 16th Workshop on*. IEEE, 2015, pp. 1–6.

[13] B. Johnson, M. Rodriguez, M. Sinha, and S. Dhople, "Comparison of virtual oscillator and droop control," in *Control and Modeling for Power Electronics (COMPEL), 2017 IEEE 18th Workshop on*. IEEE, 2017, pp. 1–6.

[14] Y. Lin, B. Johnson, V. Gevorgian, V. Purba, and S. Dhople, "Stability assessment of a system comprising a single machine and inverter with scalable ratings," in *Power Symposium (NAPS), 2017 North American*. IEEE, 2017, pp. 1–6.

[15] P. Kundur, "Power system stability and control," 1994.